Chaos

Confined direct and reverse chemical gardens: Influence of local flow velocity on precipitation patterns

I. Ziemecka (iD), F. Brau (iD), and A. De Wit (iD)

View Online   Export Citation   CrossMark

ARTICLES YOU MAY BE INTERESTED IN

AIP Publishing

Confined direct and reverse chemical gardens: Influence of local flow velocity on precipitation patterns

View Online   Export Citation   CrossMark

I. Ziemecka, (ID) F. Brau, (ID) and A. De Wit[a] (ID)

AFFILIATIONS

Nonlinear Physical Chemistry Unit, Université Libre de Bruxelles (ULB), Brussels 1050, Belgium

[a]**Author to whom correspondence should be addressed:** adewit@ulb.ac.be

ABSTRACT

Various cobalt silicate precipitation patterns can be observed when an aqueous solution of cobalt ions gets into contact with a solution of silicate ions upon injection of one solution into the other in the confined geometry of a Hele–Shaw cell. The properties of these precipitation patterns are studied here as a function of the injection flow rate, densities and viscosities of the solutions, and the choice of which solution is injected into the other one. Our results show that the structure of the precipitation pattern depends on the local velocity as well as on the difference in viscosities between the injected and the displaced solutions. Specifically, decreasing the injection flow rate and/or decreasing the density jump while increasing the difference in viscosities between the reactant solutions results in more circular patterns. Moreover, we show that some structures are robustly observed in given ranges of the local flow velocity in the cell. Locally, precipitation can then transition from one type of pattern to another during injection, according to that preferred structure at the given local velocity. We also show that injection of the cobalt solution into the silicate solution results in the so-called direct patterns that are different from the reverse patterns obtained when the silicate solution is injected in the solution of cobalt ions. Our results help in understanding the production of precipitate structures under nonequilibrium flow conditions.

Pattern formation is an ubiquitous phenomenon encountered in biological and chemical systems driven out-of-equilibrium. A very interesting example of the pattern forming systems are chemical gardens growing due to a combination of fluid dynamics and chemical reactions to produce a variety of structures. In those chemical gardens, precipitation patterns are typically formed in the wake of moving reaction fronts. When a reactant of the chemical garden recipe is injected into another one in a confined geometry, complex spatiotemporal phenomena can also occur across the precipitation zone due to gradients in density, viscosity, or permeability, for instance. Here, we analyze experimentally to what extent the structure of the precipitation pattern depends on the local flow velocity. Moreover, we analyze how the pattern can transform from one type of structure to another according to the preferred structure at the given local flow rate. Our results pave the way to a possible flow control of pattern formation in chemical garden systems.

I. INTRODUCTION

Chemical gardens are three-dimensional structures growing while a precipitation reaction between a metal salt and, for instance, a sodium silicate solution occurs. They look like growing plants, hence their name.[1–7] When a metallic salt seed is placed in a beaker containing a sodium silicate solution, it quickly dissolves while forming a semipermeable membrane. Through transport across that membrane, the water molecules further dissolve the metal salt, inducing an increase of the osmotic pressure. Beyond a given pressure, the membrane breaks which releases the salt solution that rises as a buoyant jet because it is less dense than the surrounding liquid. Further precipitation results in mineral structures that resemble growing plants. The process has already a long historical tradition since it was first described in the 17th century[8] and typically serves as an interesting experiment for school demonstrations. Not only the beauty but also the complexity of the processes involved (e.g., osmosis, reaction-diffusion, buoyancy, hydrodynamics, precipitation, etc.) make chemical gardens attractive for fundamental studies.

In that regard, the macroscopic self-organization of chemical garden tube structures is also interesting in terms of material science.[5,9–11] Moreover, since they present similarities with hydrothermal vents in the primitive ocean where the first forms of life may have appeared, chemical gardens are analyzed in connection to studies on the origin of life.[12,13]

In order to control the growth of three-dimensional chemical garden structures, recent studies have analyzed experimentally the dynamics when a metallic salt solution is directly injected into a bulk sodium silicate solution, giving the so-called "direct chemical gardens." Depending on the injection flow rate, various modes of growth have been observed.[4] The problem can be further controlled by injection of one solution into the other in confined, quasi two-dimensional Hele–Shaw cells (two Plexiglas plates separated by a thin gap).[14–18] Reduction of one of the dimensions of the reactor makes the growth dynamics more reproducible and easier to characterize. Previous experimental studies on such confined chemical gardens have investigated the effect of varying the nature of reactants (various cations and anions)[17] and the concentration of the solutions[14,18] on the resulting pattern. Strikingly, different patterns with various colors can be observed with a transition between them in the course of injection.[14] Preliminary results on "reverse gardens" obtained by injecting the silicate into the metal salt solution have further shown that direct and reverse patterns can be different even if concentrations and injection flow rate are the same,[15] similarly to what is observed in 3D tanks.[19] The effects of varying the injection flow rate and the thickness of the Hele–Shaw cell have recently been investigated by Wagatsuma et al.[18] They have shown that, depending on the flow rate, different patterns such as algaes, shells, and filaments can be observed. They have further measured the injection pressure at the injection point for the various patterns, showing that the smallest injection pressure is obtained in case of a shell pattern.

From a theoretical point of view, a mathematical model has been recently developed to describe the growth conditions of the filament pattern.[18] In parallel, it has been shown numerically for rectilinear displacements that fingering precipitation patterns can result from a precipitation reaction when the local permeability is a decreasing function of the concentration of the solid product.[20,21] The influence of buoyancy-driven instabilities[22] has also been shown numerically to control the formation of needlelike precipitate structures.[23]

However, in radial geometries, a further complexity arises from the fact that the local velocity decreases with distance from the injection point. Recent work has shown that this effect can have an influence on the spatial distribution and yield of chemical fronts.[24] The effect of changes in the local displacement velocity on the selection of the precipitation patterns and on the transition between them is still not understood. Similarly, the effect of varying the density and viscosity of the solutions remains unclear.

In this context, we study here experimentally in a confined geometry the selection of chemical garden precipitation patterns and the transition between them as a function of the local velocity in a radial displacement. We find that characteristic patterns are observed in a robust way in some ranges of local velocities. A transition between different structures can then appear at the outer rim of the pattern in the course of injection as the local velocity decreases with the distance from the injection point. We also

analyze the impact of changing the relative physical properties of the two reactant solutions or of injecting the silicate into the cobalt solution.

The article is organized as follows. We describe the experimental setup in Sec. II. In Sec. III, we characterize five distinct precipitate patterns: filaments, shells, moss, lichen, and worms observed in direct chemical gardens. In Sec. IV, the effect of injection flow rate and local velocity on the structure of the pattern and on the transition between them is presented. The effect of density and viscosity differences between solutions is addressed in Sec. V. In Sec. VI, we study reverse chemical gardens at different injection flow rates. Discussion and conclusions are in Sec. VII.

II. MATERIALS AND METHODS

The experiments are performed in the confinement of a Hele–Shaw cell composed of a large pool (35×35 cm^2) and a smaller upper plate (21×21 cm^2),[25] separated by a gap h $= 0.5$ mm, see Fig. 1. The cell is made of acrylate plates that are transparent and inert to the reactants. The pool is initially filled with solution B. A fixed volume of solution A is injected radially through an inlet in the lower plate at a fixed flow rate Q imposed by a syringe pump (kdScientific). One reactant is a sodium silicate (Na$_2$SiO$_3$) solution of pH $= 12.5$ purchased from Merck. It contains (27.0 ± 1.5) % (w/w) of SiO$_2$, which corresponds to a concentration (6.1 ± 0.3)M with respect to silica. The other reactant is a cobalt chloride (CoCl$_2$) solution of concentration 1.38M and of pH 3.4, prepared by dissolving in water the hydrated salt CoCl$_2 \cdot$ H$_2$O (Sigma-Aldrich).

In a series of so-called "direct" experiments, 0.5 ml of cobalt chloride solution A is injected into the pool initially filled with the sodium silicate solution B at a flow rate Q varying from 0.05 μl/s to 110 μl/s. The same Q ranges are studied for the reverse experiment where 1 ml of sodium silicate solution A is injected into cobalt chloride solution B. It should be noted that the cell gap is open to the pool and the injected volume of solution A can push solution B, initially present between the two plates, out to the pool. The setup is illuminated from both below and above by light pads, and the experiments are recorded from above using a digital camera (PixeLINK B742U). In some experiments, saccharose has been added to the CoCl$_2$ solution to bring it to the same density as the silicate solution. Densities and viscosities of the various solutions used are summarized in Table I.

III. PRECIPITATION PATTERNS
A. Morphology of patterns

When a CoCl$_2$ solution is injected into a Na$_2$SiO$_3$ solution at a constant flow rate Q (direct case), a precipitation reaction occurs in the contact zone. Different morphologies of patterns are observed: filaments,[14,17] shells,[18] moss and lichen (these two structures being gathered under the term "algaes"[18]), and worms as shown in Fig. 2.

Filaments typically have a pink color and a tubular structure as seen in Fig. 2. They grow initially as one or more tubes with small, tortuous segments. The shell morphology is made of repeated, arc-shaped precipitate. During the growth of a new segment, a change of color of the already existing segments is observed. Those different
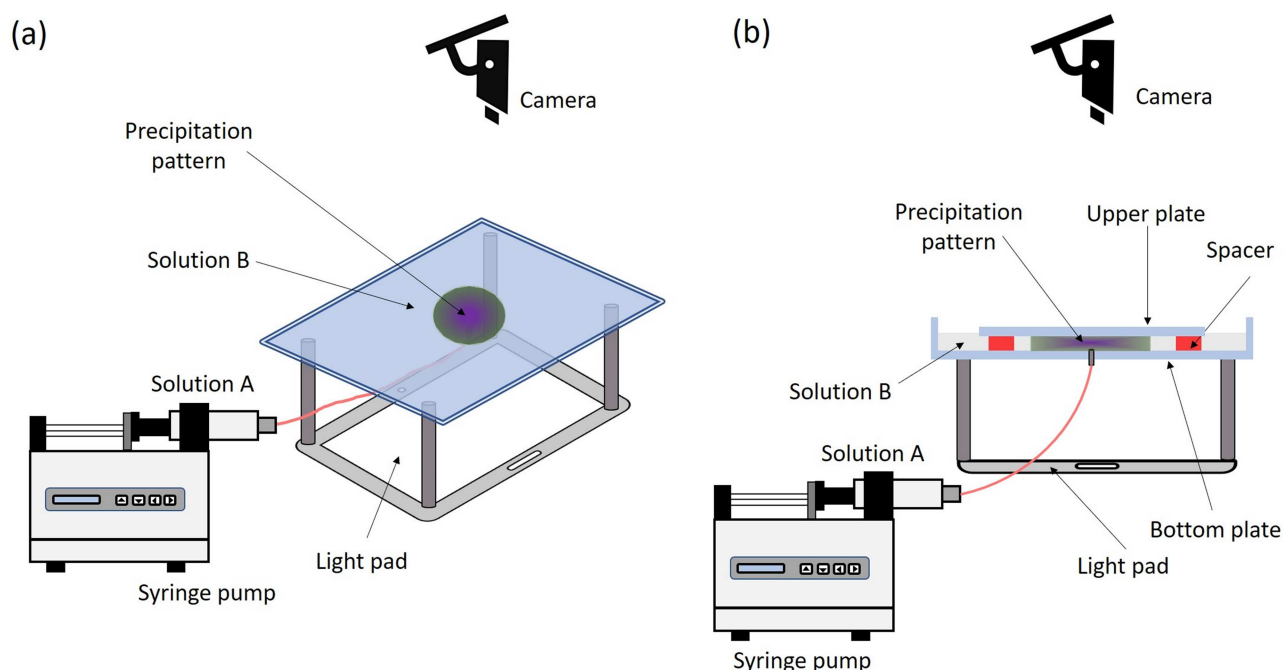
FIG. 1. Schematic representation of the Hele–Shaw cell seen (a) from the top and (b) from the side.

colors (i.e., pink, violet, blue, and green) suggest different chemical compositions,[15,26] but this is difficult to check as the current setup does not allow to sample the precipitate without destroying it. Out of all observed morphologies, the shells appear to be the most brittle ones as they are the only ones in which cracking is observed as seen in Fig. 3.

The moss morphology (Fig. 2) has the features of compact fibers. It grows symmetrically from the injection point creating a circular pattern of violet-blue color with large inner fingers. It appears to be the most circular and symmetric of all the patterns. The lichen structure also has a green-violet color, but this color is here more pronounced. Lichens grow rather symmetrically but, as opposed to moss, have segmented structures. Because they are obtained at low flow rates, the time during which the lichen structure develops is very long, up to a few hours. In the course of time, the structure of lichen changes to another type of structure that has a morphology of short, violet rain-worms (Fig. 2).

B. Pattern characterization

In order to characterize quantitatively the observed patterns, we define different quantities, see Fig. 4.

The radius R_{max} of the pattern is the distance from the injection point to the most distant point of the pattern. The area A_p is the area inside the pattern perimeter. We characterize the pattern by calculating its deviation from circular growth,[25] $d = A_p/(\pi R^2_{max})$ where d varies from 0 to 1 with 1 meaning that the pattern is perfectly circular.

The variation of d and R_{max} for each of the four observed patterns is presented in Figs. 4(b) and 4(c). The lowest value around 0.1 of the circular deviation d is observed for the filaments, which also feature a fast growing value of R_{max}. The value of d increases in time for shells and has its maximum values for the moss structures that grow in a compact way with a roughly circular symmetry around the injection point. For the lichen, d has a lower value than for moss but still a larger d than for filaments and shells.

TABLE I. Physical properties of the various solutions used. Viscosity is measured at 24 °C with a Brookfield Viscometer. Density is measured at 24 °C with a DMA 35, Anton Paar Density Meter.

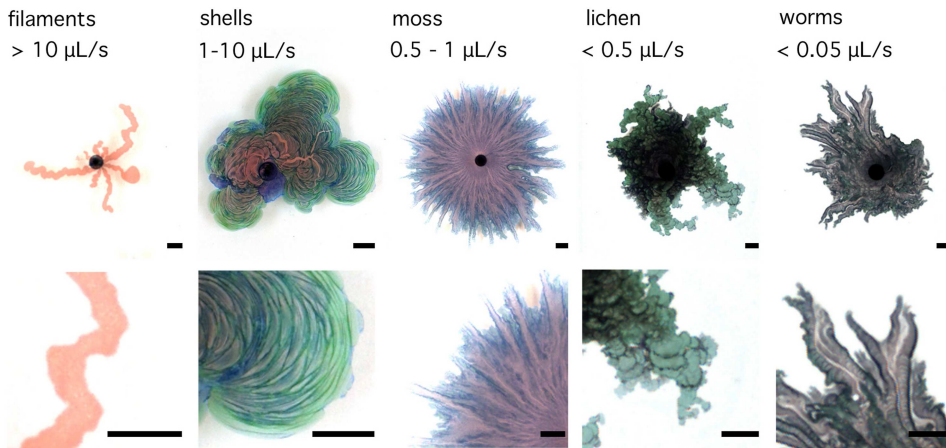| Solution		Concentration (mol/l)	Viscosity (mPa s)	Density (g/ml)
Na_2SiO_3 solution	Sodium silicate solution (Merck)	6.1	63.0 ± 3.0	1.39 ± 0.05
$CoCl_2$ solution	$CoCl_2 \cdot 6H_2O$ (Sigma-Aldrich)	1.38	1.81 ± 0.01	1.15 ± 0.05
$CoCl_2$ solution, containing 70 g of saccharose in 100 ml (70 w/v%)	$CoCl_2 \cdot 6H_2O$ (Sigma-Aldrich), saccharose	1.38 2.04	100.0 ± 7.0	1.38 ± 0.05

FIG. 2. Direct precipitate patterns observed close to the inlet at different flow rates when the $CoCl_2$ solution is injected into the Na_2SiO_3 solution. The scale bar is 5 mm. The lower row shows a zoom on a subpart of the upper row picture.
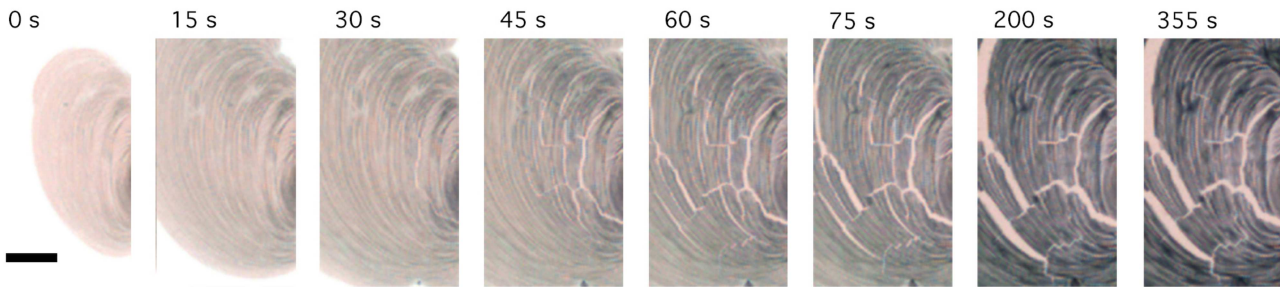

FIG. 3. Change of color and cracking of a shell pattern during $CoCl_2$ solution injection. The scale bar is 5 mm.
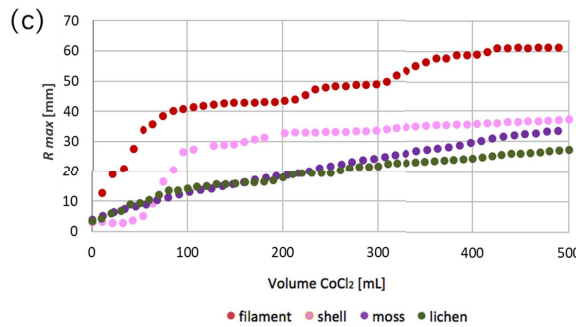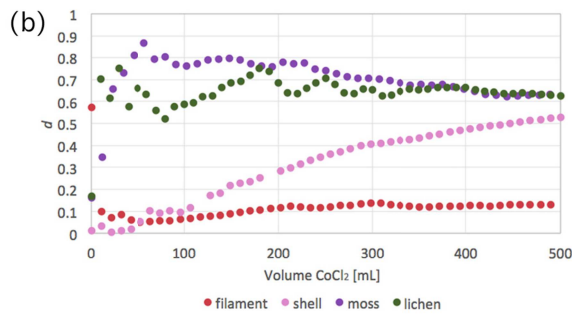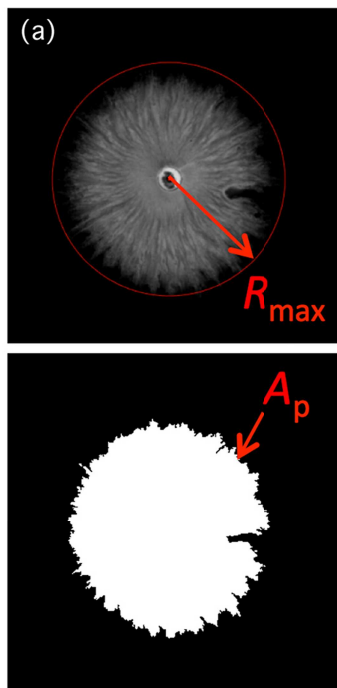

FIG. 4. (a) Quantities used for pattern characterization: the radius R_{max} of the circle passing by the furthest distance of the pattern from the injection point and the area A_p inside the pattern perimeter, used to compute the pattern density $d = A_p/(\pi R^2_{max})$. Evolution of (b) d and (c) R_{max} for various patterns as a function of the volume of $CoCl_2$ solution injected.
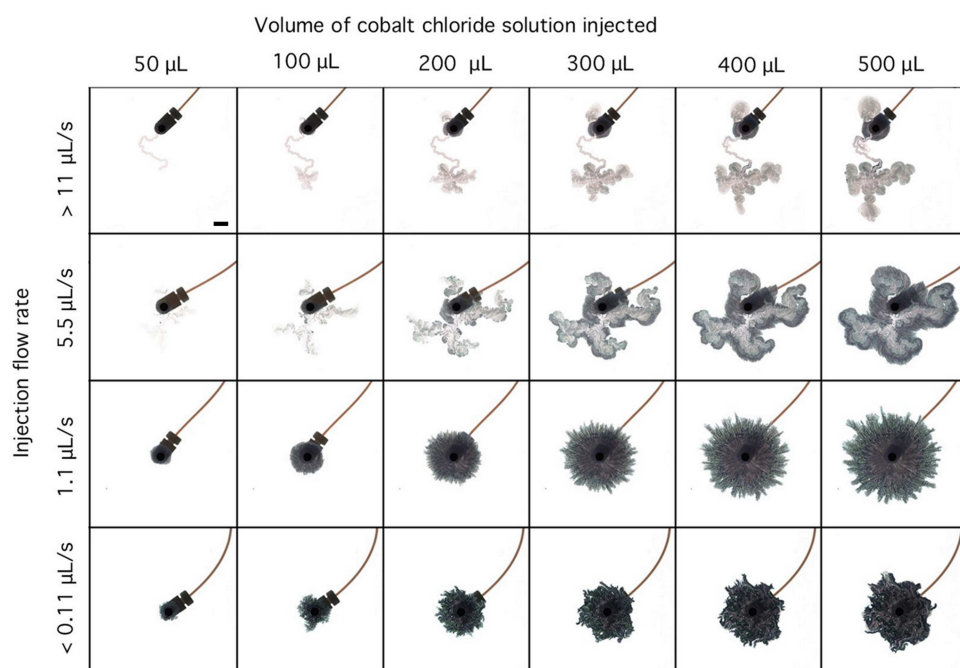
Volume of cobalt chloride solution injected

FIG. 5. Evolution of direct precipitation patterns for different injection flow rates as a function of the volume of CoCl$_2$ injected. The scale bar is 5 mm.

IV. EFFECT OF INJECTION FLOW RATE AND LOCAL VELOCITY

We find that, within a range of injection flow rates Q, some morphologies are favored close to the injection inlet (Fig. 2). For Q above 10 μl/s, filaments are the first pattern to be seen at the entrance of the injected reactant in the cell. On the contrary for a flow rate between 1 and 10 μl/s, shells grow first. For Q between 0.5 and 1 μl/s, we obtain right away the so-called moss structure at the inlet. For 0.05 < Q < 0.5 μl/s, we get a pattern named lichen while, at the lowest flow rates below 0.05 μl/s, we observe shapes similar to worms. At the beginning of the injection, we thus see that one type of morphology is preferred depending on the value of the constant flow rate applied. Let us refer to this pattern as the favored morphology for that imposed flow rate of injection.

Because the liquid is injected radially at constant Q, the local velocity U = Q/(2πhr) decreases with the distance r from the injection point because of the radial expansion. Also, locally, the velocity can sometimes decrease because of a physical barrier caused by the presence of a precipitate. The first observed pattern then stops to grow, and the characteristic pattern typically stable for lower Q starts developing. This change in pattern morphology during the course of the experiment is presented in Figs. 5 and 6.

We can observe that, depending on the evolution in the radial distance and thus on the local change in velocity, filaments continue at a certain point to grow as shells [Figs. 5 and 6(a)]. Similarly, beyond a given radius from the injection point, shells become moss [Figs. 5 and 6(b)], moss turns into lichen [Figs. 5 and 6(c)], or lichen into worms [Figs. 5 and 6(d)]. The growth of lichen takes hours, and studies of their subsequent evolution into even slower growing worm patterns are at the limit of our setup because of blocking

precipitation around the injection valve for such low displacement velocities.

The growth of the pattern as a function of the volume of CoCl$_2$ injected for a fixed Q is shown in Fig. 5. Note that we prefer here to compare experiments at the same injected volumes of displacing solution and not at the same time because the actual time of the experiments goes from a few seconds up to a few hours depending on the value of Q. As seen in the two first columns of Fig. 5, the favored morphology develops first. However, because of radial injection and as the precipitate forms a barrier between the two fluids, the local displacement velocity of the liquids decreases and the second pattern, preferred at lower local speeds, is next observed.

Sometimes, two or three different patterns develop successively, probably due to an asymmetric precipitation that slows down the speed of the material locally. As an example, Fig. 7(a) shows the cogrowth of shells and moss appearing simultaneously as the first patterns for a global flow rate where typically shells are the favored regime. Later on, classical successive transitions from shells to moss and eventually to lichen are observed [Fig. 7(b)]. Note that cogrowing patterns are then always those obtained for lower local velocities, i.e., we obtain then the favored pattern for the imposed Q and the preferred structure for a lower local velocity if, locally, the precipitation slows down the flow. The decrease of the local velocity explains thus the transition from one preferred pattern to another when the radial distance from the injection point increases as well as the possible cogrowth of two or three patterns when geometrical asymmetries locally slow down the flow. The type of favored morphology is thus imposed by the local velocity and not by the global injection flow rate.
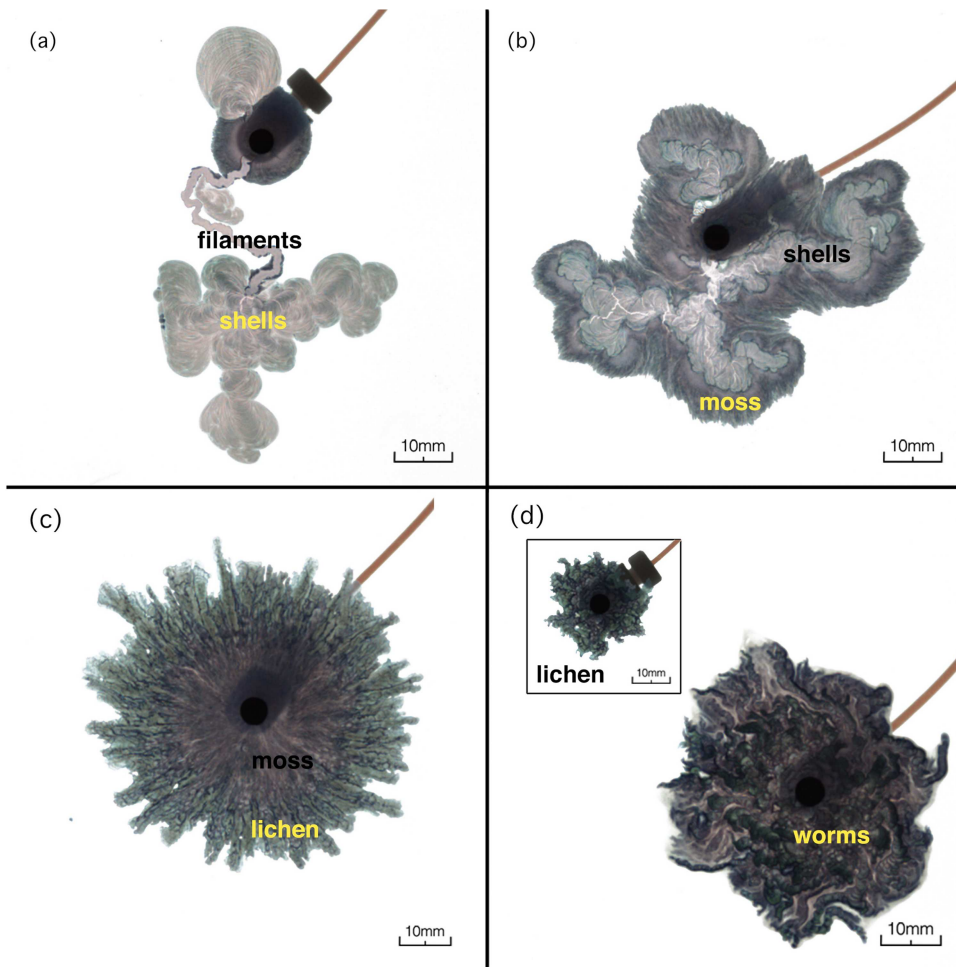
FIG. 6. Transition between various patterns during the course of one experiment: Switch from (a) filaments to shells, (b) shells to moss, (c) moss to lichen, and (d) lichen to worms (inset: image at the earlier time to better highlight the lichen structure).
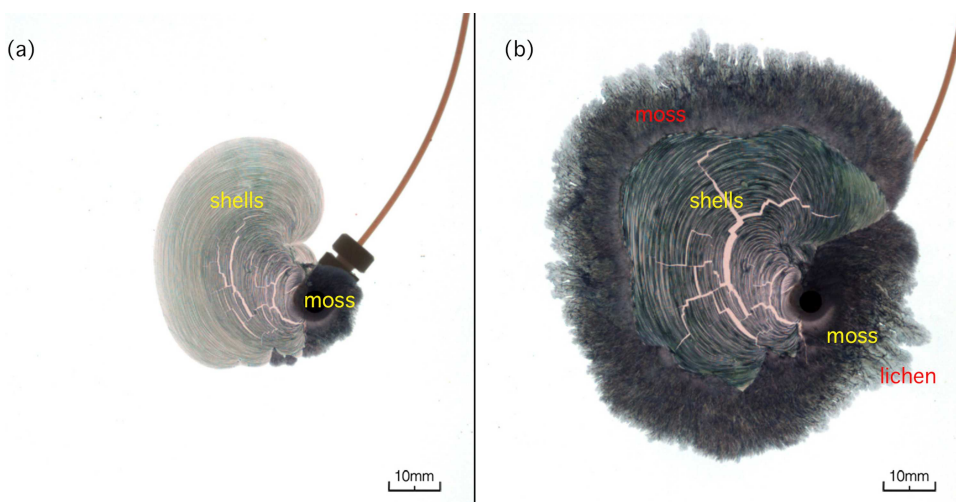

FIG. 7. Cogrowth of shells and moss for the same injection flow rate due to (a) two different local velocities at the same radius depending on local solid obstacles or (b) a decrease of the local flow rate when the distance from the injection point increases.
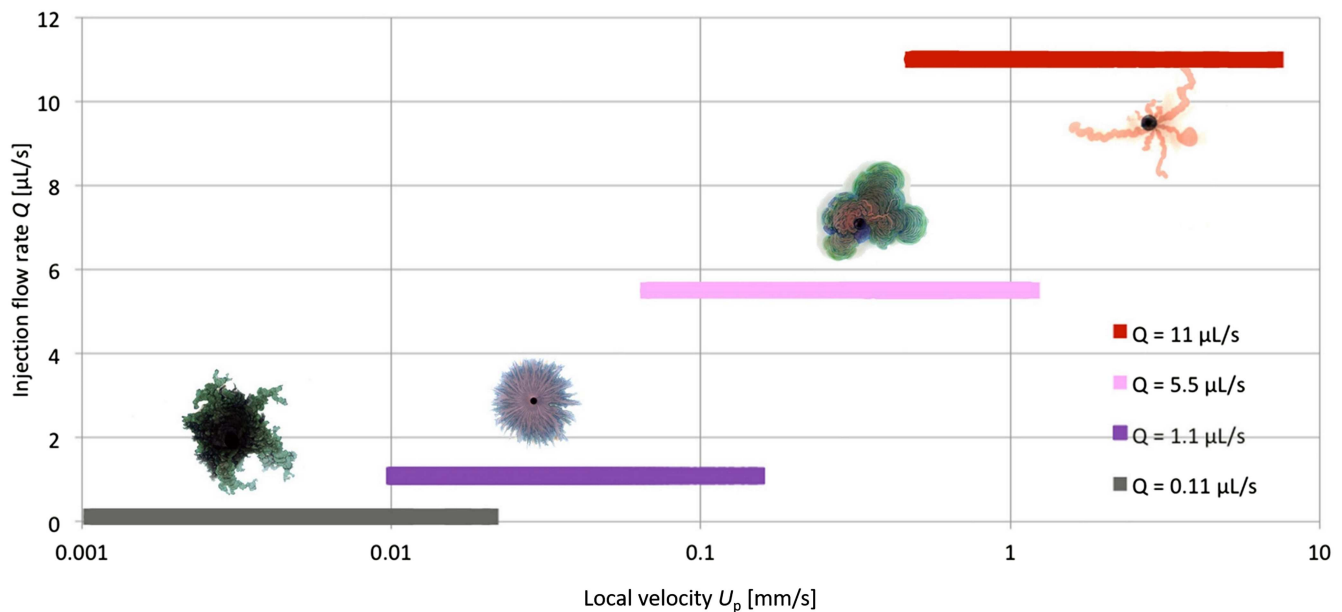
FIG. 8. Typical favored patterns for the different flow rates used and range of the local velocities at the pattern periphery, $U_p = Q/(2\pi hR_{max})$, in which they are observed.

In Fig. 8, a correlation between the injection flow rate Q and the possible local velocity at a given radius R_{max} during the experiment is presented. The horizontal colored bars show the range of local speeds $U_p = Q/(2\pi hR_{max})$ at which the given morphology is observed. At a large Q, U_p is initially large, and filaments are obtained. As R_{max} increases, U_p cascades down and the related preferred pattern is then observed in the cell for all corresponding U_p as shown in the figure. As Fig. 8 shows, for some U_p ranges, two different morphologies can be observed depending on the history of the pattern growth.

V. EFFECT OF VARYING THE SOLUTION DENSITY AND VISCOSITY

To verify the influence of a density and viscosity difference between the two reacting solutions on the pattern formation, the same experiments were performed using a $CoCl_2$ solution the density of which has been adjusted by the addition of saccharose to match the density of the sodium silicate solution. As seen in Table I,

the $CoCl_2$ solution becomes then more viscous than the silicate one. The typical morphologies observed in this isodense but reverse viscosity ratio situation for different injection flow rates are presented in Fig. 9. We observe filaments, a mixture of filaments and moss, moss and lichen but all structures are now much more circular as the injected solution is now more viscous.

For a large flow rate ($>10\,\mu l/s$), a structure like filament is observed. However, in this case, these filaments are growing symmetrically and circularly from the injection point. The larger the flow rate, the larger the number of filaments and the more compact their structure [Fig. 10(a)].

Close to the inlet, the filaments are very packed, while further away from the inlet, they have more space and the arms of filaments are hence more distanced from each other. Lower flow rates give an opposite result, see Figs. 10(a) and 10(b). The filaments behave then similarly to the structures obtained when the solutions have different densities: after a decrease of the local flow rate, the filaments undergo a transition to the structure favored at lower speeds, in this case into moss. We observe that, when the experiment is finished,

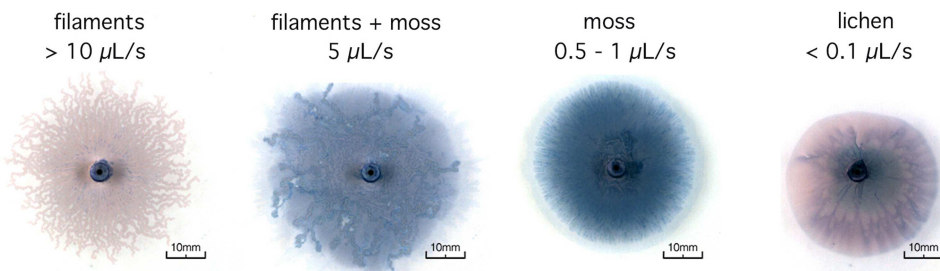| filaments	filaments + moss	moss	lichen
> 10 μL/s	5 μL/s	0.5 - 1 μL/s	< 0.1 μL/s

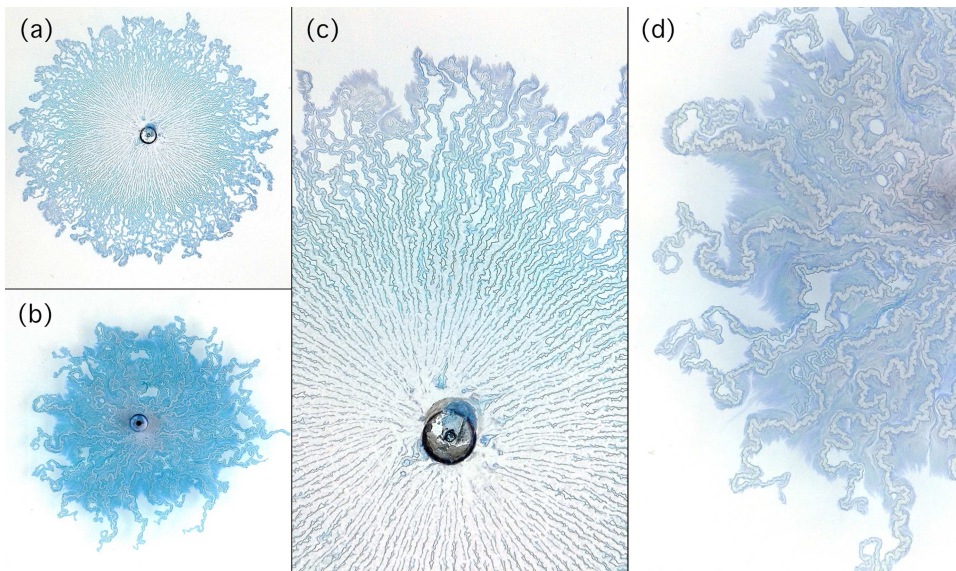FIG. 9. Direct precipitate patterns observed for different flow rates when both solutions have the same density.

FIG. 10. Filament structures when the two reactant solutions have the same density, obtained at a flow rate of Q = (a) 110 μl/s and (b) 11 μl/s. (c) Zoom on panel (a) showing the very compact center of the filament pattern that allows moss to grow only around the tips of the filaments. (d) Zoom on panel (b) evidencing that, as there are fewer filaments at a lower flow rate, the moss can grow all along the filaments in the middle of the less compact structure.

the filaments are overgrown by moss, i.e., the moss grows, filling the available space between the filaments. Where the filaments are very compact, the moss is prevented to grow, see Fig. 10(c). In that case, the moss grows at the end of filaments. When the structure of filaments is less compact, the moss eventually fills every available space, like in Fig. 10(d).

For the lower injection flow rates (between 1 and 10 μl/s), filaments and moss grow simultaneously almost at the same time.
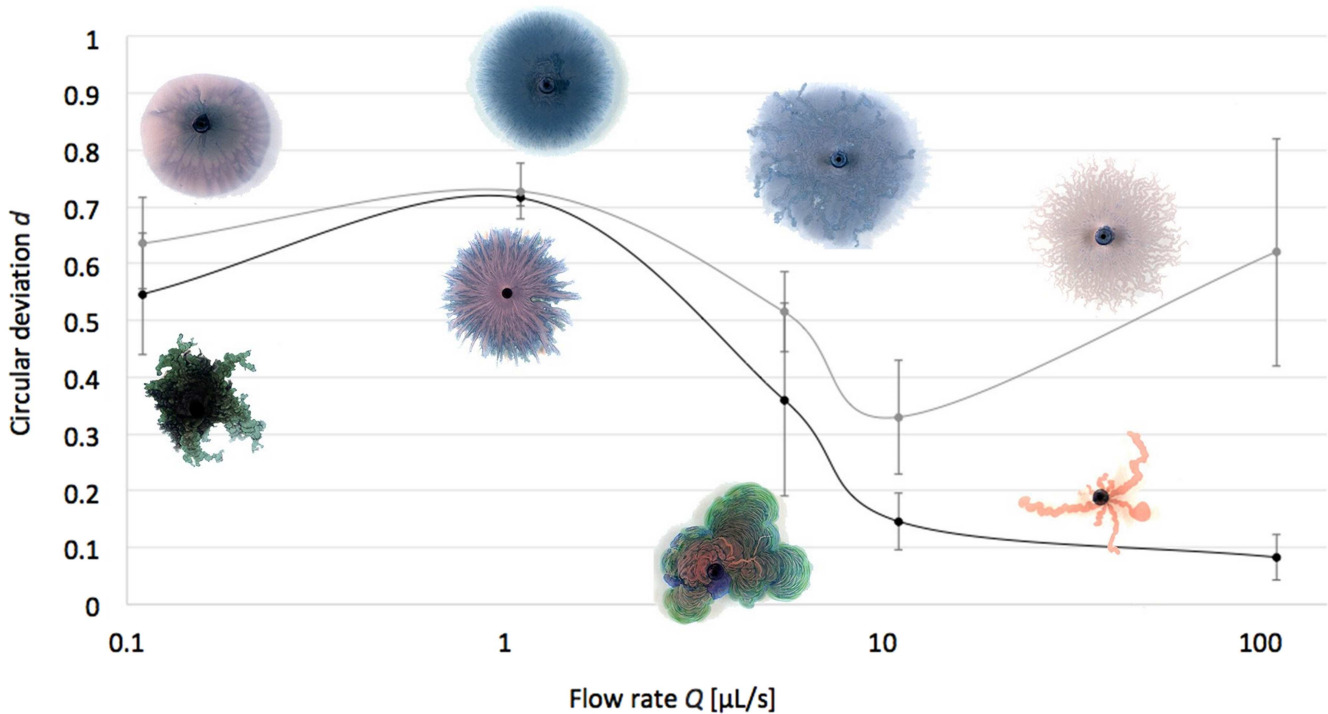

FIG. 11. Comparison of the average deviation d from the circular growth of direct patterns as a function of the injection flow rate for reacting solutions that have either different (black curve) or the same (gray curve) densities. The curves are drawn to guide the eyes. The error bars show the range of values obtained in three repeated experiments.
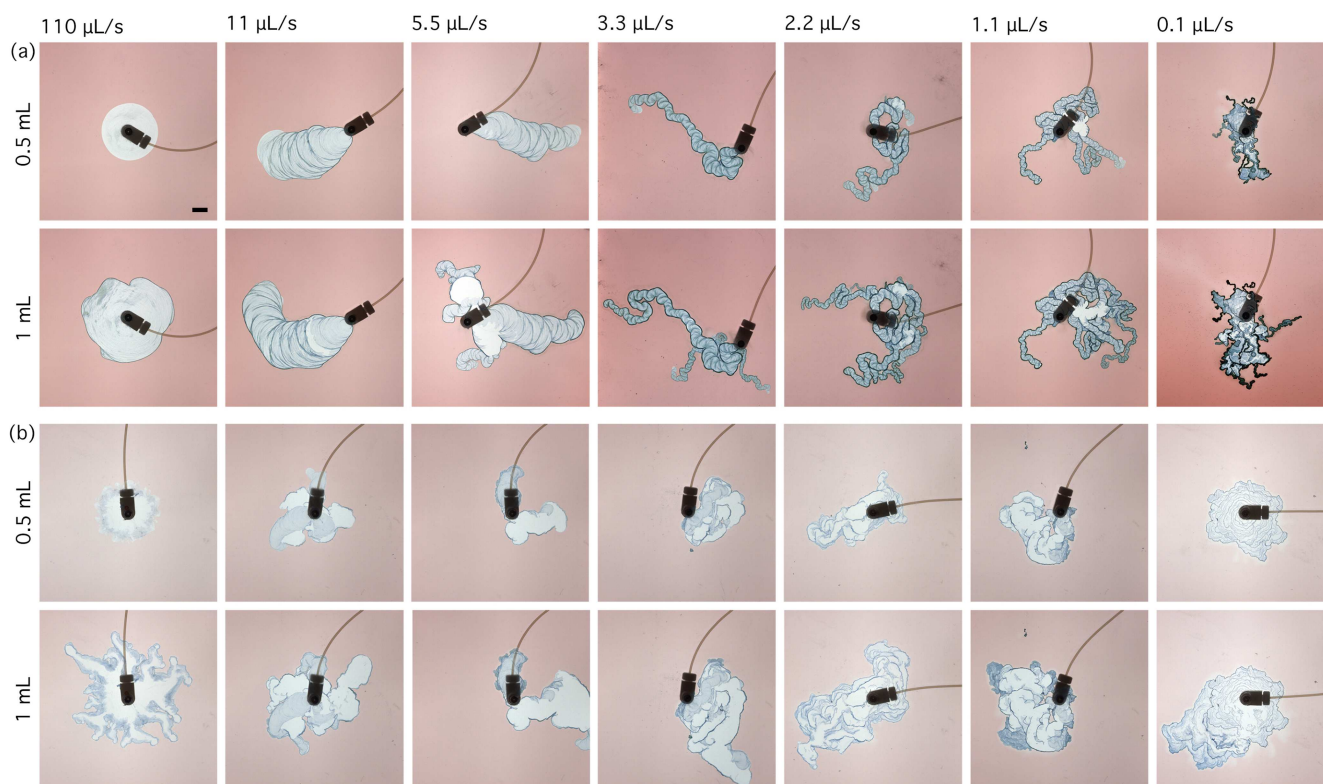
FIG. 12. Reverse chemical garden patterns observed for different flow rates after injection of 0.5 and 1 ml of sodium silicate inside a cell initially filled with $CoCl_2$ when the two solutions have either (a) different or (b) the same densities. The scale bar is 1 cm.

However, the growth of filaments is faster. The ratio of the filament to moss areas within the whole pattern decreases with the injection flow rate such that, at the low flow rates between 0.5 and 1 μl/s, it is possible to observe a structure of only moss or of moss with one filament. At the lowest flow rate of injection, a different structure, which can be considered a symmetric analog of the lichen structure, is then obtained. It is very compact and features visible segmentations in its circular structure.

Except for filaments, we observe that, for all other patterns, the structures are more circular and feature thus larger values of d when the densities of the solutions are the same, but the displacement is viscously stable (Figs. 9 and 11).

This shows that on the contrary in the direct case, injecting the less viscous solution into the more viscous silicate favors a morphologically unstable interface between the two fluids and this deformation increases when the injection flow rate is increased. Similar observations were reported by Haudin and De Wit,[16] who investigated the interplay between viscous and precipitation-driven fingering in direct chemical garden systems when injecting cobalt chloride solutions of variable concentrations into sodium silicate. This shows that the density and viscosity of the solution has an influence on the pattern morphology.

VI. REVERSE CHEMICAL GARDENS

To investigate the impact of the choice of which one of the reactant solutions is injected into the other one, we have also studied reverse chemical garden patterns obtained when the sodium silicate solution is injected into the cobalt chloride solution at the same injection flow rates as for the direct cases. Figure 12 shows these reverse patterns for different flow rates after injection of 0.5 ml and 1 ml of silicate, for solutions of either the same or different densities. Reversing the order of injection changes the density, the viscosity, and the pH gradients along the flow.

In this reverse case [Fig. 12(a)], the patterns have a white color with a blue edge that becomes darker with time. For a very large flow rate ($Q = 110 \mu$l/s), a symmetric, round flowerlike structure is observed. At lower Q, longer, tubular structures with marked segments are rather obtained. Remarkably, the lower the Q, the smaller the diameter of the tubes. During injection, the silicate makes a jet of solution that solidifies at the surface in the contact with the cobalt ion solution. This jet meanders through the other solution to form a tube. At some point, the tube stops to grow while the liquid silicate is further injected. This solution breaks through the already created wall and then meanders through the cobalt solution leading to the creation of another tube. This process repeats until the end of the injection. The number of tubes eventually obtained and the amount
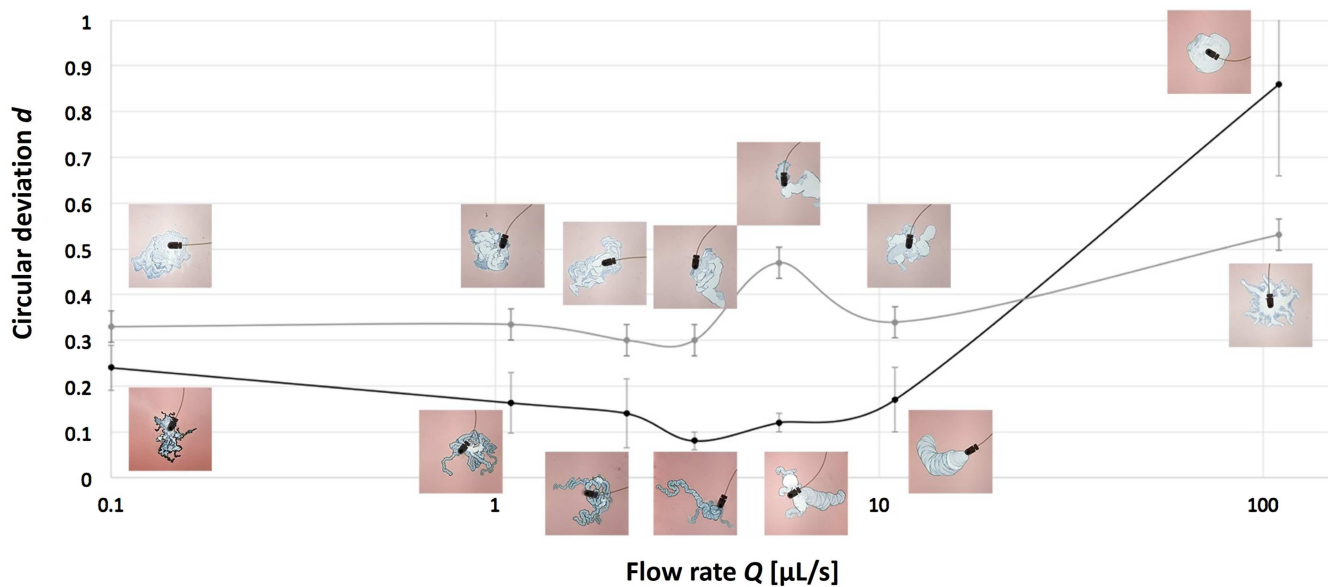
FIG. 13. Comparison of the average deviation from the circular growth d of reverse patterns as a function of the injection flow rate for reacting solutions that have either different (black curve) or the same (gray curve) densities. The curves are drawn to guide the eyes. The error bars show the range of values obtained in three repeated experiments.

of blue color are correlated to the injection flow rate: the lowest the flow rate, the larger the number of tubes and the more pronounced the blue color. This is related to the fact that, at low flow rates, more molecules have time to react which results in more blue precipitate in the wall of the structure.

The reverse patterns obtained using solutions of the same density are presented in Fig. 12(b). The structures are also white with blue edges, but their morphology is closer to flowers than to worms. We recall that the silicate solution is less viscous than the isodense $CoCl_2$ solution with saccharose, which explains that the reverse patterns are fingered at high flow rates.

The average deviation from the circular growth calculated from the same experiment repeated three times is given in Fig. 13.

The tendency is the same whether the two solutions have the same or a different density: the highest value of d is obtained for the structures formed at the largest Q. The isodense patterns have, however, a smaller d than those obtained from different density solutions because the viscosity ratio is now unfavorable.

VII. DISCUSSION AND CONCLUSIONS

We have experimentally investigated the influence of changes in the injection flow rate on the selection of chemical garden precipitates in a Hele–Shaw cell both when the cobalt solution is injected into the silicate one (direct case) and in the reverse case. We have, moreover, analyzed the differences in morphology when the density and viscosity of one reactant solution are varied.

For direct chemical gardens, various patterns such as filaments, shells, moss, lichen, and worms are obtained. We find that, depending on the local velocity, some structures are favored. For instance,

filaments are the pattern privileged at large local velocities while moss or worms are seen at intermediate and low local velocities, respectively. As, in radial geometries, the local speed decreases along the radius, this induces a transition in space in the course of the experiment from filaments to shells to moss to lichen and eventually to worms when starting from large flow rates and letting the pattern expand radially. The local flow rate affects not only the morphology but also the color of the precipitate. At this stage, it is impossible to know whether this results from a change in the oxidation state of the ions or because of a change in the crystal structure as we cannot extract a sample of the solid pattern in the cell during the experiment without perturbing the whole system. Nevertheless, this points to the possibility of controlling the targeted pattern as well as the transitions between different structures depending on the local velocity for a given fixed global injection flow rate.

Different patterns are obtained for the direct and reverse cases, confirming the fact that the order in which a solution is injected into the other matters for the selection of the spatiotemporal distribution and composition of the precipitate. For the reverse chemical gardens, the molecular composition between the structures is less diverse as the patterns are all typically white with blue edges but the injection flow rate controls the spatial structure by favoring a different diameter of the tubes building that structure. Furthermore, the morphology of the precipitates depends on both the direct and reverse chemical gardens on the relative density and viscosity between the two reactant solutions.

Our results show the large variety of different precipitate patterns that can be obtained when a precipitation reaction takes place in flow conditions. Our analysis has contributed to define some of

the key parameters that can be used for the controlled production of different materials in out-of-equilibrium conditions.

ACKNOWLEDGMENTS

REFERENCES

[1] T. Hazlehurst, J. Chem. Educ. **18**, 286 (1941).

[2] R. D. Coatman, N. L. Thomas, and D. D. Double, J. Mater. Sci. **15**, 2017 (1980).

[3] J. H. E. Cartwright, J. M. Garcia-Ruiz, M. L. Novella, and F. Otalora, J. Colloid Interface Sci. **256**, 351 (2002).

[4] S. Thouvenel-Romans and O. Steinbock, J. Am. Chem. Soc. **125**, 4338 (2003).

[5] R. Makki, L. Roszol, J. J. Pagano, and O. Steinbock, Philos. Trans. R. Soc. Lond A **370**, 2848 (2012).

[6] L. M. Barge *et al.*, Chem. Rev. **115**, 8652 (2015).

[7] M. R. Bentley, B. C. Batista, and O. Steinbock, J. Phys. Chem. A **120**, 4294 (2016).

[8] J. R. Glauber, *Furni Novi Philosophici* (Fabel, Amsterdam, 1646).

[9] J. J. Pagano, T. Bansagi, Jr., and O. Steinbock, Angew. Chem. Int. Ed. **47**, 9900 (2008).

[10] R. Makki and O. Steinbock, J. Am. Chem. Soc. **134**, 15519 (2012).

[11] C. Batista and O. Steinbock, J. Phys. Chem. C **119**, 27045 (2015).

[12] M. J. Russel and A. Hall, J. Geol. Soc. **154**, 377 (1997).

[13] L. M. Barge, I. J. Doloboff, L. M. White, G. D. Stucky, M. J. Russell, and I. Kanik, Langmuir **28**, 3714 (2012).

[14] F. Haudin, J. H. E. Cartwright, F. Brau, and A. De Wit, Proc. Natl. Acad. Sci. U.S.A. **111**, 17363 (2014).

[15] F. Haudin, J. H. E. Cartwright, and A. De Wit, J. Phys. Chem. C **119**, 15067 (2015).

[16] F. Haudin and A. De Wit, Phys. Fluids **27**, 113101 (2015).

[17] F. Haudin, V. Brasiliense, J. H. E. Cartwright, F. Brau, and A. De Wit, Phys. Chem. Chem. Phys. **17**, 12804 (2015).

[18] S. Wagatsuma, T. Higashi, Y. Sumino, and A. Achiwa, Phys. Rev. E **95**, 052220 (2017).

[19] J. J. Pagano, T. Bansagi, Jr., and O. Steinbock, J. Phys. Chem. C **111**, 9324 (2007).

[20] Y. Nagatsu Y. Ishii, Y. Tada and A. De Wit, Phys. Rev. Lett. **113**, 024502 (2014).

[21] P. Shukla and A. De Wit, Phys. Rev. E **93**, 023103 (2016).

[22] F. Haudin, L. A. Riolfo, B. Knaepen, G. M. Homsy, and A. De Wit, Phys. Fluids **2**, 044102 (2014).

[23] G. Potari, A. Toth and D. Horvath, Chaos **29**, 073117 (2019).

[24] F. Brau, G. Schuszter, and A. De Wit, Phys. Rev. Lett. **118**, 134101 (2017).

[25] G. Schuszter, F. Brau, and A. De Wit, Phys. Chem. Chem. Phys. **18**, 25592 (2016).

[26] J. H. E. Cartwright, B. Escribano, and C. I. Sainz-Diaz, Langmuir **27**, 3286 (2011).